

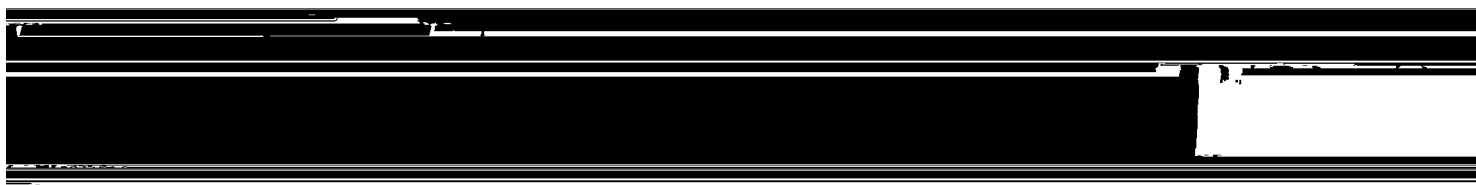
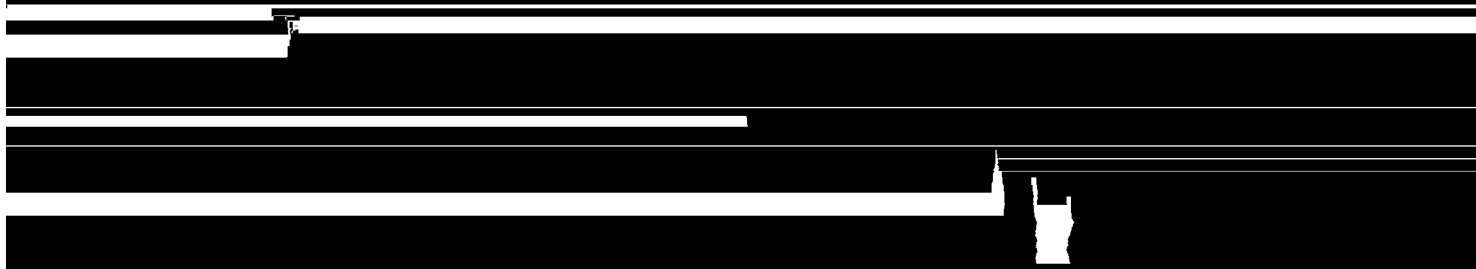
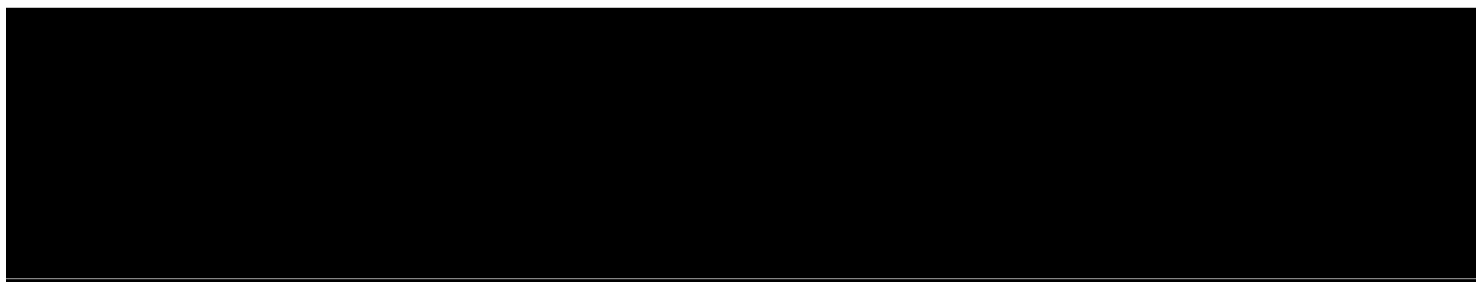
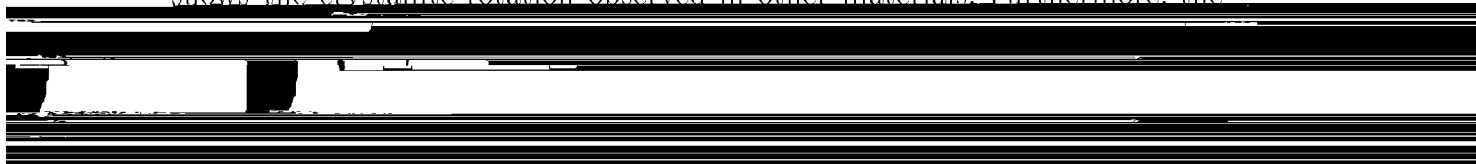
Anhydride–Polyacrylonitrile Mixture

Michael M. Degen, Nicola Costanzino, John Bechhoefer¹

Department of Physics, Simon Fraser University, Burnaby, BC V5A 1S6, Canada

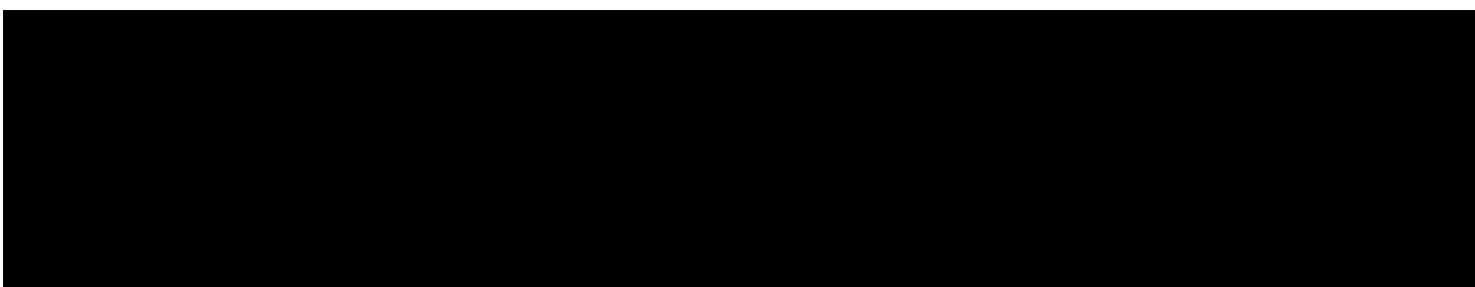
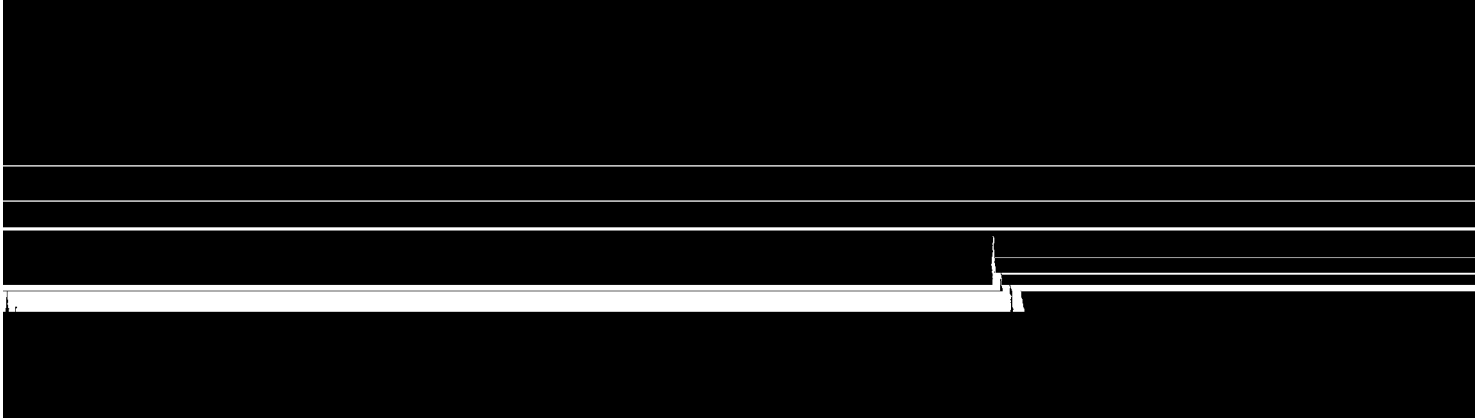
These materials show typical band spacings of $500\ \mu\text{m}$ or less. Recently, Lagasse and coworkers have observed band spacings on the order of 10 mm, over an order of magnitude larger than seen before. The material studied was a blend of a low-molecular-weight organic solvent, maleic anhydride, and a small amount of the polymer polyacrylonitrile[9,10].

Lagasse et al. studied this blend using wide-angle and small-angle X-ray scattering. They also studied the polyacrylonitrile foams remaining after removing the maleic anhydride by sublimation. Their studies confirm that this blend shows the crystallite rotation observed in other materials. Furthermore, the

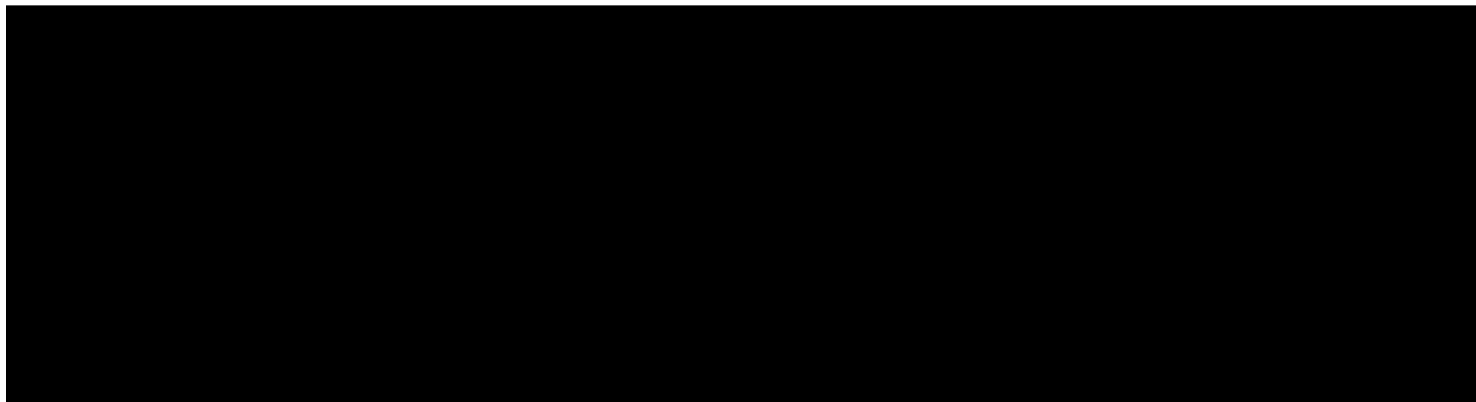
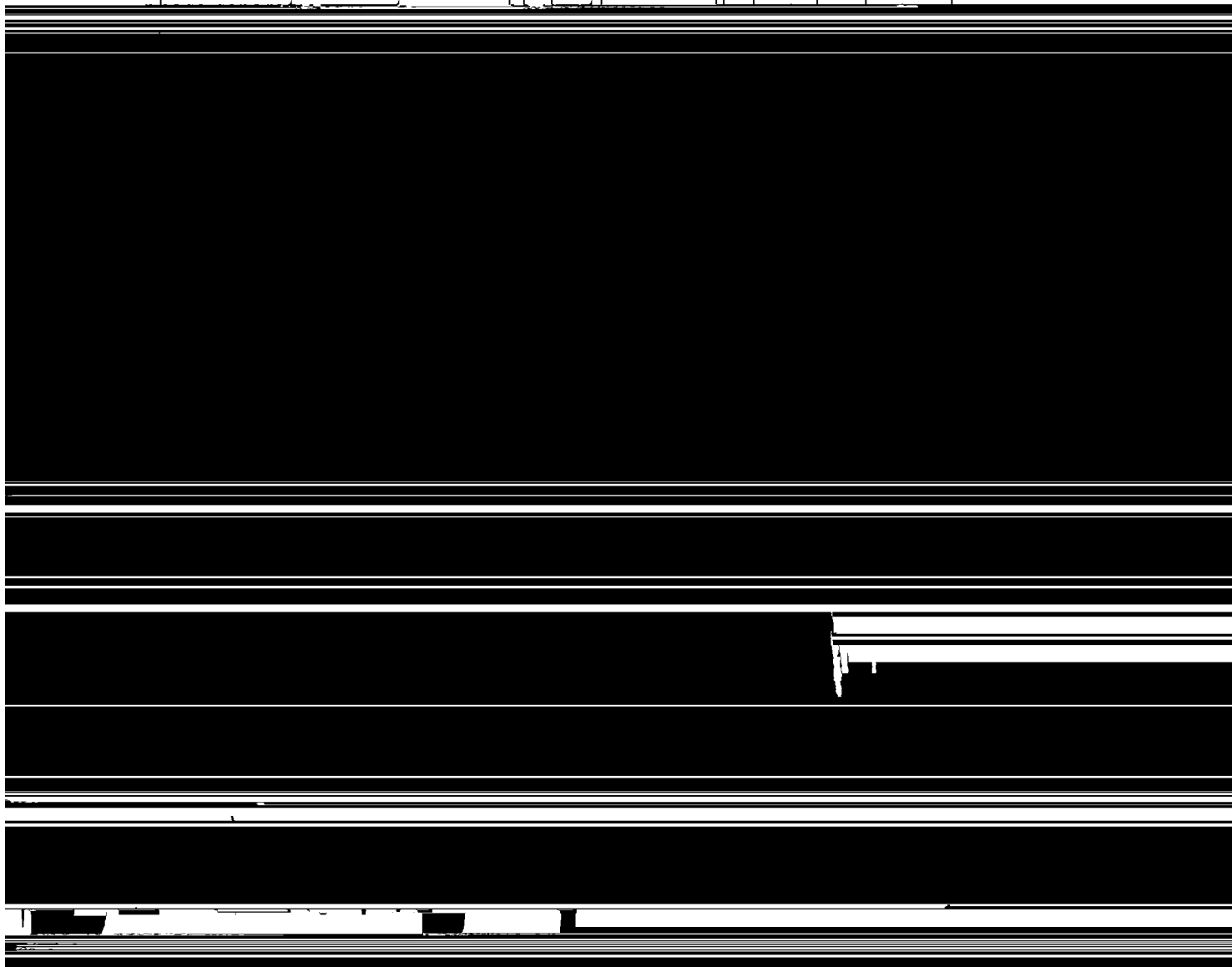


have side walls at least twice as thick as the bottoms, ensuring unidirectional heat flow.

The temperature of the melt is measured via a thermistor immersed directly in it. Once the melt has cooled to the desired ΔT , the glass cover plate is



depending on how completely the polyacrylonitrile is dissolved prior to cooling[11]. In all of the measurements reported here, we first completely dissolve the polymer. Repeating the measurements using different melting and cooling protocols gave the same band spacings and front velocities. Furthermore, stirring the melt after the phase separation and before nucleation is induced has no measurable effect on the banded spherulites. Thus, we conclude that the



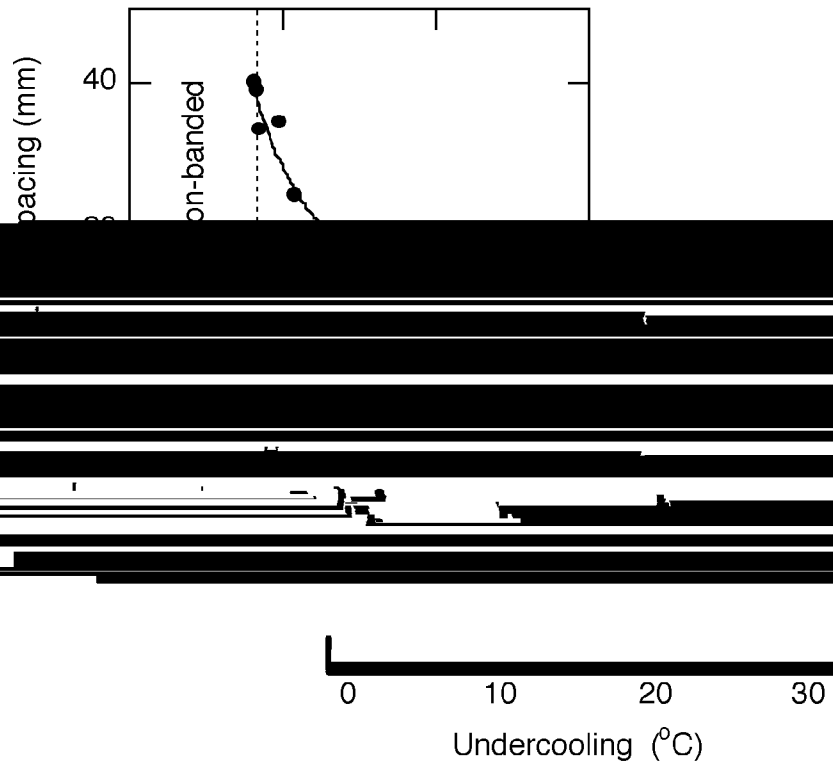


Fig. 1. (a) Band spacing vs. Undercooling. The solid curve is a fit with $\lambda \propto \Delta T^{-1.5}$.
 $\lambda \propto \Delta T^{-1.5}$. The choice of exponent is prompted by a model due to Owen[13].

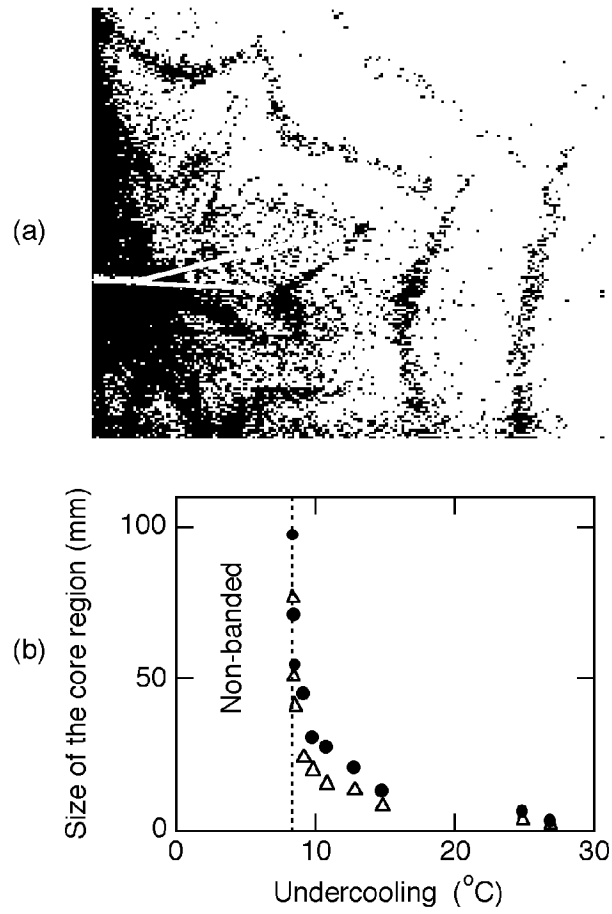


Fig. 2. (a) Photograph showing the core region and first few bands of a banded spherulite grown at $\Delta T = 24.9^\circ\text{C}$. The probe used to induce nucleation is visible on the left side of the image and two lines indicate the relevant distances to the first band. (b) Size of the core region versus undercooling. (—) Data from the photograph in (a).

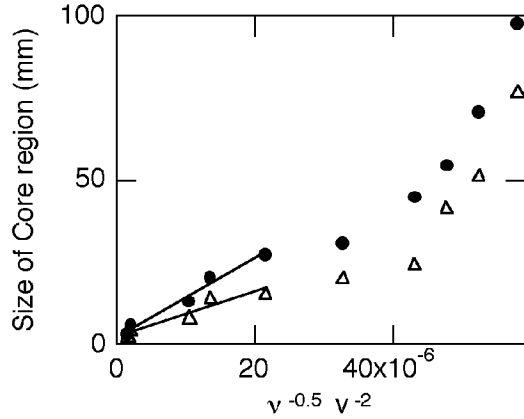


Fig. 3. Size of the core region vs. Tiller's scale factor. (●) denotes the maximum and (Δ) the minimum. The solid lines serve as guides to the eye and indicate the region where Tiller's model appears to be most applicable.

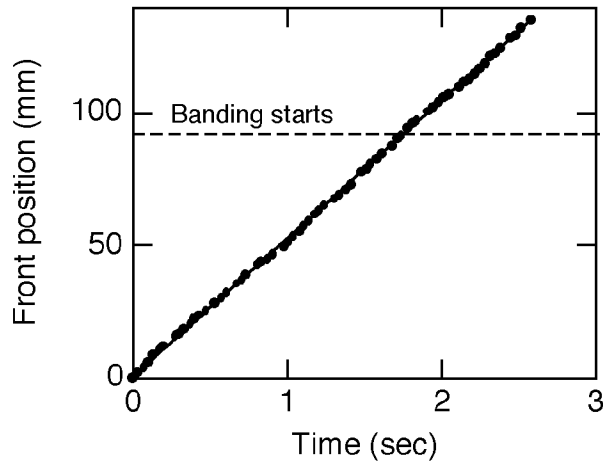


Fig. 4. Position of solidification front vs. Time at $\Delta T = 8.3^\circ\text{C}$. Specific origins of position and time are arbitrary, although near the nucleation site. The dashed line indicates the position of the first dark band. No change in slope is noticeable in the graph.

in Fig. 3. The solid lines in Fig. 3 show that the model qualitatively accounts for the behavior in the high velocity, or high undercooling, region. However, the model does not predict a divergence of the core region and thus fails near the undercooling threshold ($\Delta T = 8.3^\circ\text{C}$).

3.3 The Solidification Front.

[REDACTED]

[REDACTED]

[REDACTED]

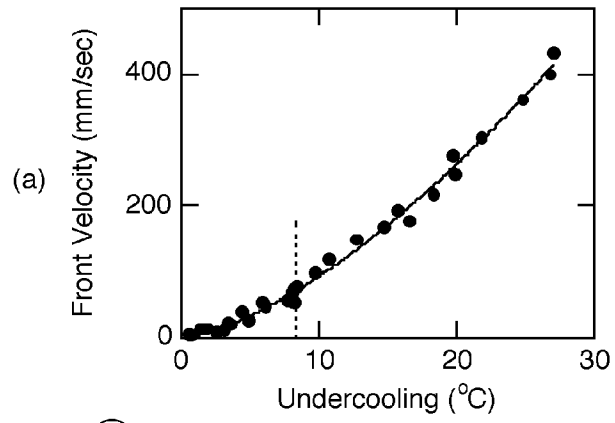
[REDACTED]

[REDACTED]

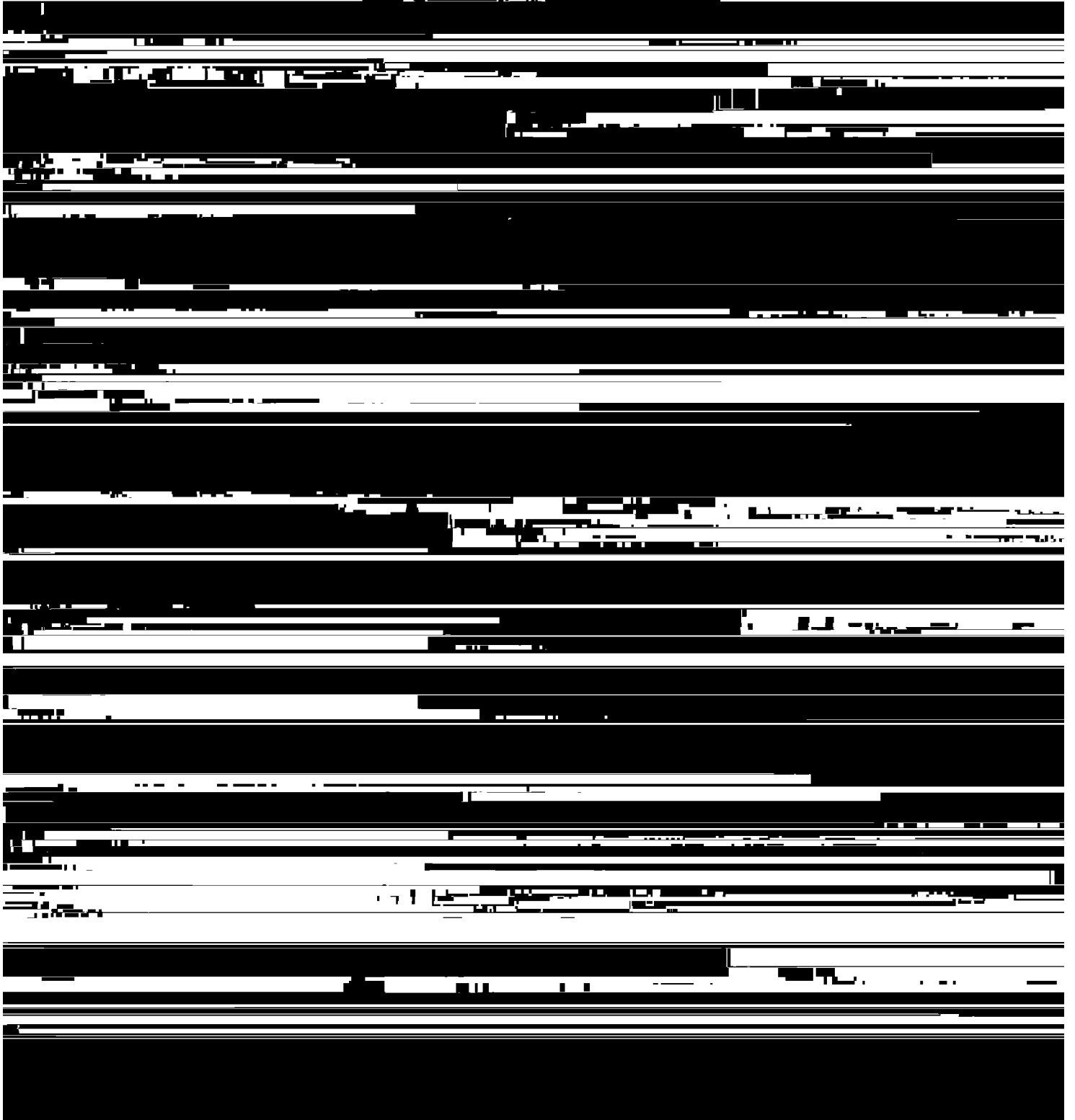
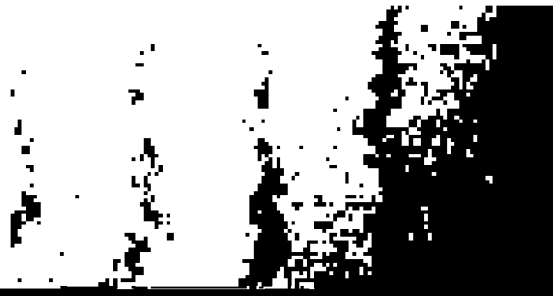
[REDACTED]

[REDACTED]

[REDACTED]



(a)



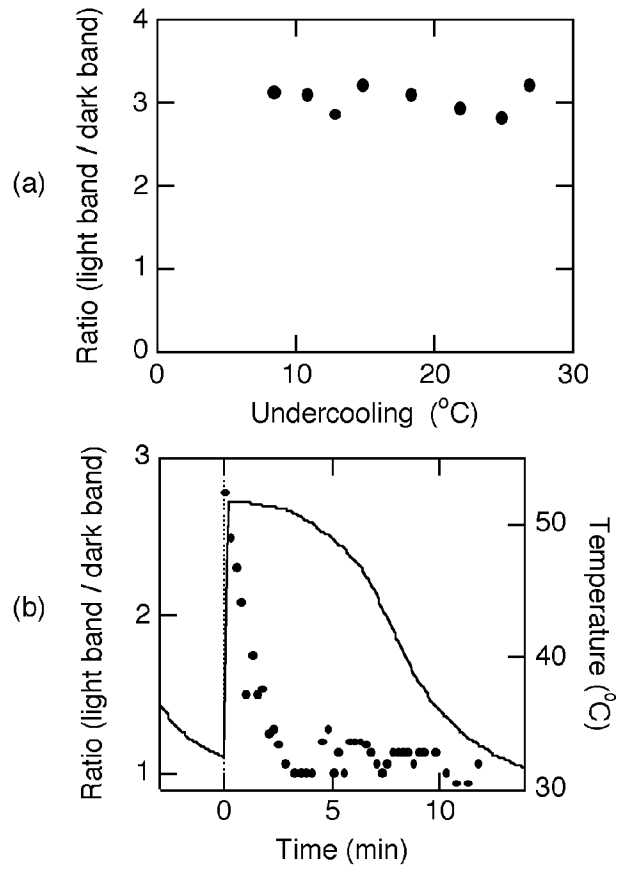


Fig. 8. (a) Ratio of the sizes of the light band to the dark band vs. Undercooling. Measurements were taken immediately after passage of the solidification front. (b)

[Redacted text line]

[Large redacted block]

[Redacted text line]

[Redacted text line]

[Redacted text line]

[Redacted text line]

[Redacted text line]

[Redacted text line]

[Redacted text line]

[Redacted text line]

[Redacted text line]

[Redacted text line]

[Redacted text line]

[Redacted text line]

[Redacted text line]

[Large redacted block]

[Large redacted block]

[Redacted text line]

[Redacted text line]

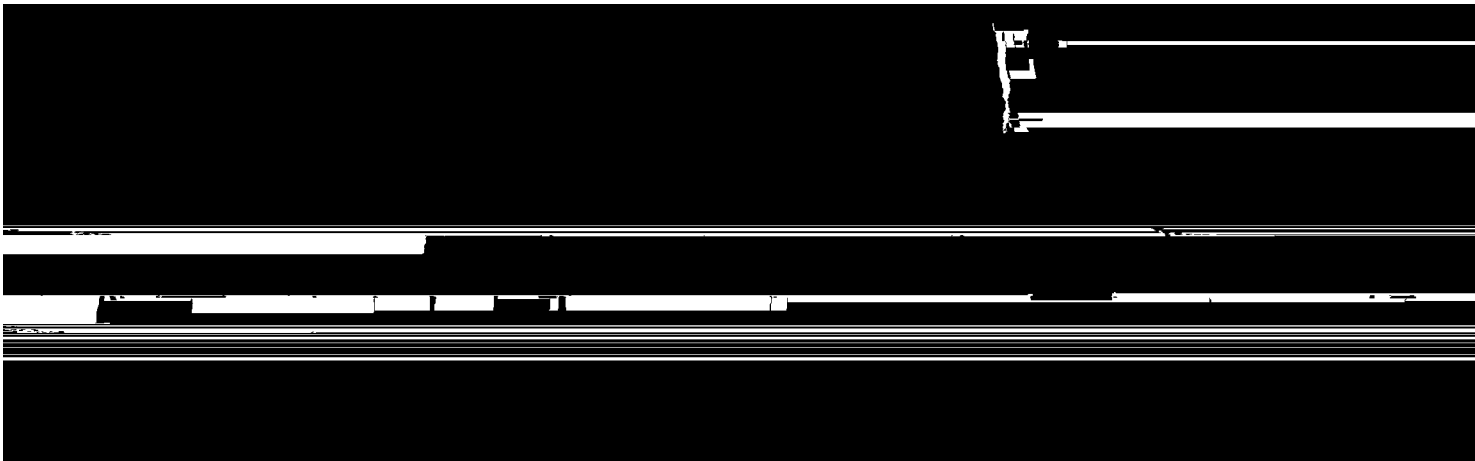
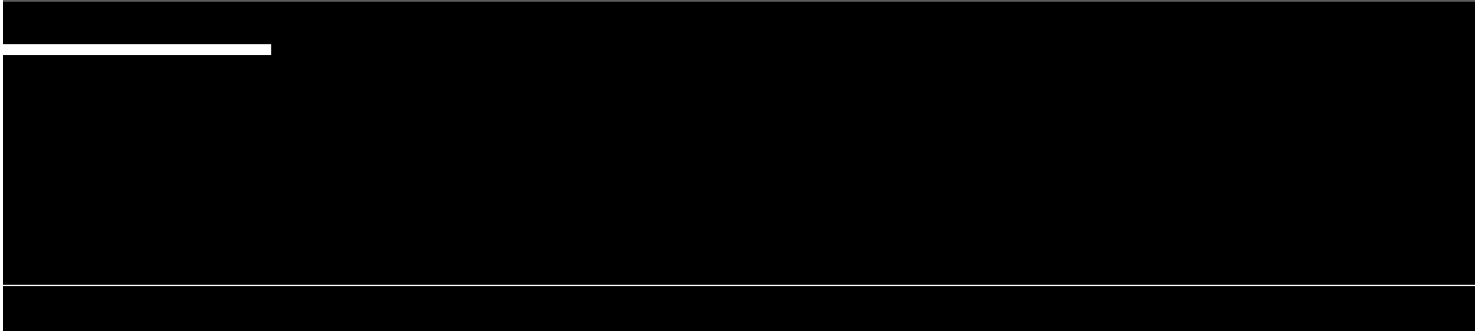
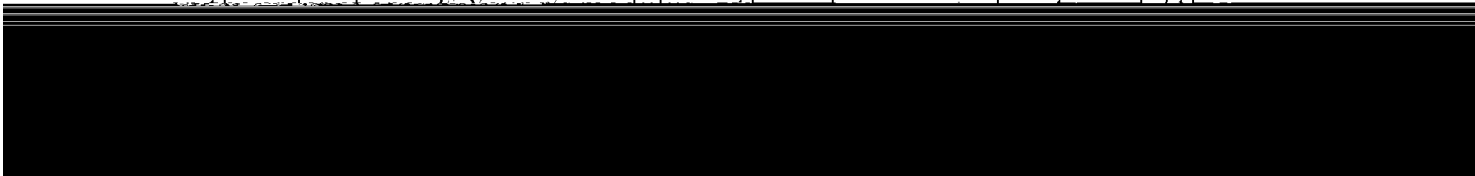
[Redacted text line]

[Large redacted block]

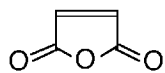
[Redacted text line]

[Redacted text line]

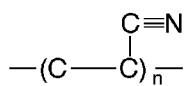
energies and argues that $\lambda = A(E/\sigma)^{0.5} d^{1.5}$ with A being a geometrical factor



(a)



(b)



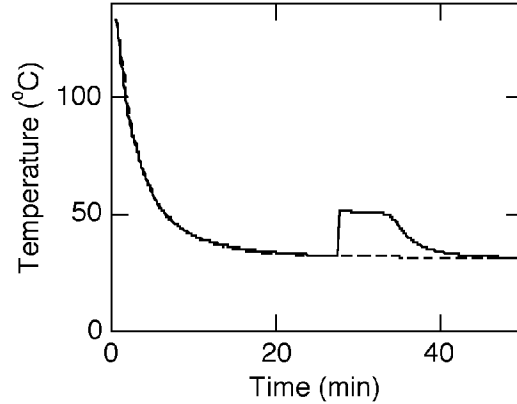


Fig. 10. A typical cooling curve. The dotted curve is an extrapolation of the initial cooling, and the shaded region represents the additional latent heat released during freezing.

of heat loss through the mold to the temperature stage is calibrated using cooling curves of hot water, which has a known c_p . Next, the initial cooling in Fig. 10 is fit with a double exponential, shown as the dashed curve, which indicates two separate time scales are present in the cooling. The first time scale is on the order of ≈ 1 min and is associated with heating of the silicone

mold by the hot melt, as shown by varying the initial temperature of the mold. The second time scale is on the order of ≈ 10 min and is the heat loss through the mold to the temperature stage. From this rate of heat loss and the mass of the mixture, we calculate $c_p = 1.8 \pm 0.2$ J/°C gm. We calculate L from the “extra” area between the actual cooling curve and the extrapolated initial cooling, indicated by the shaded region in Fig. 10. This method yields $L = 100 \pm 15$ J/gm.

We have also measured the viscosity of the melt using a capillary tube viscometer[27]. The viscosity is found to obey the Andrayde-Eyring equation $\nu = \nu_o e^{T_o/T}$, with $\nu_o = 0.07 \pm 0.01$ cS and $T_o = 1580 \pm 60$ K[28].

References

- [1] H.D. Keith and F.J. Padden Jr., Banding in polyethylene and other spherulites, *Macromolecules* **29** (1996) 7776–7789.
- [2] A. Keller, The spherulitic structure of crystalline polymers. Part I. Investigations with the polarizing microscope, *J. Poly. Sci.* **17** (1995) 291–308.
- [3] D.C. Bassett, Polymer morphology: Pure and applied, *J. Macromol. Sci.–Phys. B* **35** (1996) 277–294.

- [5] J.L. Hutter and J. Bechhoefer, Many modes of rapid solidification in a liquid crystal, *Physica A* **239** (1997) 103–110.
- [6] J.L. Hutter and J. Bechhoefer, Three classes of morphology transitions in the solidification of a liquid crystal, *Phys. Rev. Lett.* **79** (1997) 4022–4025.
- [7] J. Bechhoefer and J.L. Hutter, Morphology transitions in a liquid crystal, *Physica A* **249** (1998) 82–87.

[8] J. Bechhoefer, G. B. L. ...

- [19] M. Scandola, G. Ceccorulli, M. Pizzoli and M. Gazzano, Study of the crystal phase and crystallization rate of bacterial poly(3-hydroxybutyrate-co-3-hydroxyvalerate), *Macromolecules* **25** (1992) 1405–1410.
- [20] T.L. Cheng and A.C. Su, Spherulites of long-chain branched cis-1,4-polybutadiene, *Macromolecules* **26** (1993) 7161–7166.
- [21] V. Balsamo, F. von Gyldenfeldt and R. Stadler, Thermal behavior and spherulitic superstructures of SBC triblock copolymers based on polystyrene (S), polybutadiene (B) and a crystallizable poly(ϵ -caprolactone) (C) block, *Macromol. Chem. Phys.* **197** (1996) 3317–3341.
- [22] D.C. Bassett, Lamellae and their organization in melt-crystallized polymers, *Phil. Trans. Roy. Soc. London* **A348** (1994) 29–43.
- [23] K.L. Singfield, J.K. Hobbs and A. Keller, Correlation between main chain chirality and crystal “twist” direction in polymer spherulites, *J. Cryst. Growth* **183** (1998) 683–689.
- [24] H.D. Keith and F.J. Padden, Jr., Ringed spherulites in polyethylene, *J. Polym. Sci.* **31** (1958) 415–421.